

## Highlights

### **Large-Scale Calorimetry Time Response Characterization and Correction**

Giovanni Di Cristina, Erik Johnsson, Eric Mueller, Matthew Bundy, Anthony Hamins

- A series of 4 m to 6 m Douglas fir tree fires were characterized by measuring the transient mass burning rate, radiative emission, and heat release rate.
- The fires grew extremely fast, obtaining peak heat release rates (HRR) from about 7 MW to 42 MW within 7 s to 10 s.
- A methodology is presented on rescaling the transient calorimetry heat release rate to correct for the system time response, using relatively fast instruments including a strain gauge type load cell and water-cooled heat flux gauges.
- The calculation results showed the two rescaling methods yielded peak HRR values within 15 % of each other on-average.

# Large-Scale Calorimetry Time Response Characterization and Correction

Giovanni Di Cristina<sup>a</sup>, Erik Johnsson<sup>a</sup>, Eric Mueller<sup>a</sup>, Matthew Bundy<sup>a</sup>, Anthony Hamins<sup>a,\*</sup>

<sup>a</sup>*Fire Research Division, National Institute of Standards and Technology, Gaithersburg, MD, USA*

---

## Abstract

Recent fire experiments testing 4 m to 6 m tall Douglas fir trees pushed the limits of the time response of the National Institute of Standards and Technology (NIST) large fire calorimeter due to their fast fire growth. The fires obtained peak heat release rates from 7 MW to about 42 MW within 7 s to 10 s. The calorimetry system is dependent on multiple instruments each with their own time response. Calibration experiments with imposed square wave thermal pulses have characterized the system time constant as approximately 8 s. Consequently, the time response becomes a significant source of uncertainty in the transient results. Utilizing measurements from fast-responding mass load cell and far-field radiometers as models for the heat release rate (HRR) response, a methodology is developed to rescale the transient HRR to correct for the calorimetry system's time response. The results from each correction method are compared to each other and the oxygen consumption HRR. Although both methods have different limitations, their respective results agree within 15% of each other, on average. This study provides insight on the accuracy and uncertainty of oxygen consumption calorimetry systems.

*Keywords:* Calorimetry, tree fires, Metrology, Time Response, Uncertainty

---

## 1. Introduction

The heat release rate (HRR) of a fire is a key measurement as it is directly related to fire behavior, growth, and hazard. Thus HRR is critical for characteriz-

---

\*Corresponding Author

*Email address:* `anthony.hamins@nist.gov` (Anthony Hamins)

ing and modeling fires [1]. Oxygen ( $O_2$ ) consumption calorimetry [2] allows fire researchers to quantify the HRR of a fire. By analyzing the combustion products and measuring the temperature, gas flow, and gas concentrations (mainly oxygen), the energy release rate of a fire can be determined. Considering how crucial HRR measurements are, considerable efforts have been taken to reduce the measurement uncertainty of  $O_2$  consumption calorimetry systems [3–6]. These efforts have resulted in improvements to the uncertainties related to the air mass flow, instrument drift, the heat of combustion per unit mass of oxygen, and corrections for the effects of carbon monoxide. However, the system response time is usually not addressed, in large part due to the complexity of deconvoluting the response and delay times of the many measurements that make up the HRR determination.

There are few papers in the literature that identify or attempt to address this issue. Lyon and Abramowitz used an integral technique to remove the effect of instrument response time on peak and integrated heat release rate values measured using the Ohio State University (OSU) apparatus for various materials [7]. Messerschmidt and van Hees presented helpful discussions on the effect of response times on oxygen consumption calorimetry and provided guidance on acceptable response times [8]. Pitts considered time response effects in the characterization of the HRR of a commercial flexible polyurethane foam in the cone calorimeter. Mathematical forms for the HRR were posited and the resulting rescaled HRRs were determined [9]. Croce proposed several methods to correct the calorimeter time response. The sampling and analysis system was characterized to determine its response and the data was then used to deconvolute the measured gas concentration history, providing a more accurate representation of the actual gas concentration profile [10]. Bryant et al. characterized and corrected HRR transients in square-wave shaped thermal pulses of natural gas fires by using the heat flux profile from a distant radiometer [11]. This study extends the work of Bryant by comparing correction methods using two types of sensors for rapidly growing fires.

The National Institute of Standards and Technology (NIST) calorimetry system is composed of various types of instruments,<sup>1</sup> each with their own time response. Although corrections are made for instrument delay and lag times, the NIST calorimetry system does not specifically correct for system time response [5]. The ASTM standard for large-scale calorimetry recommends treating the system

---

<sup>1</sup>Certain equipment, instruments, software, or materials, commercial or non-commercial, are identified in this paper in order to specify the experimental procedure adequately. Such identification does not imply recommendation or endorsement of any product or service by NIST, nor does it imply that the materials or equipment identified are necessarily the best available for the purpose.

response time as an additional lag time because the correction for response time is rather complicated and the argument goes that for response times relatively fast compared to the time for fire development, the difference in the results is small [12]. The NIST large-scale calorimetry system has a time constant of approximately 8 s based on analysis of imposed square-wave shaped changes to the thermal load during calibration experiments using a 20 MW natural gas burner [5]. However, considering that the peak HRRs of the fires investigated in this study occurred in less than 10 s after ignition and the entire duration of flaming combustion was about 30 s to 40 s, the system response time becomes a significant source of uncertainty in the transient results.

Calorimetry measurements in a rapidly growing fire are especially challenging. This is also true for fires in which the volumetric generation rate of exhaust gases is on the same order as the exhaust system extraction rate. In such a case, there may be a build-up of exhaust gases in the canopy hood, where gas products will mix, leading to additional system response time. This was the case in the fires studied here for which the maximum practical exhaust flow was used. A transient smoke layer was observed indicating that mixing of combustion products occurred. In contrast to calorimetry systems, water-cooled heat flux gauges and mass load cell systems commonly used in fire research are relatively fast. Heat flux gauges have time constants of about 450 ms or faster, whereas mass load cells have response times typically on the order of 1 ms.

A method to correct for the system time response is developed and presented in this study. The total heat released calculated from the calorimetry system is rescaled using the data from two types of fast-responding instruments (heat flux gauge and mass load cell), leveraging the idea that the total heat released determined by calorimetry over the entire experimental duration is invariant. The resulting rescaled HRR profiles yield peaks that are narrower than the original and exhibit faster times to obtain the peak HRR. Each method relies on strong assumptions about the instrumentation and fire dynamics. However, this approach provides a way to estimate the actual HRR and a methodology to correct for system time response in relatively large and rapidly growing fires.

## **2. Experimental Setup**

Six Douglas fir (*Pseudotsuga menziesii*) tree fire experiments were conducted under the NIST large-scale calorimeter exhaust hood which has a 13.8 m by 15.4 m footprint [5]. The trees ranged from 3 m to 6 m tall, with the trees' foliage having an average wet basis moisture content of about 9 %. The six trees were selected for

Table 1: Tree specimen descriptions including the height and maximum width, the initial tree mass corrected for water, and the measured tree foliage moisture content on a wet basis ( $MC_w$ ). The combined expanded uncertainties are listed in the table and are equal to  $\pm 3.0$  cm for the lengths.

Tree	Height [m]	Width [m]	Initial Dry Mass [kg]	$MC_w$ [%]
1	3.37	2.35	$14.38 \pm 0.57$	$7.3 \pm 1.9$
2	3.66	2.15	$18.47 \pm 0.57$	$7.8 \pm 2.0$
3	4.23	2.71	$27.67 \pm 0.57$	$7.9 \pm 2.0$
4	4.08	2.55	$24.46 \pm 0.57$	$7.7 \pm 2.0$
5	5.77	2.79	$54.93 \pm 0.57$	$9.9 \pm 2.6$
6	5.81	3.13	$49.48 \pm 0.57$	$11.5 \pm 3.1$

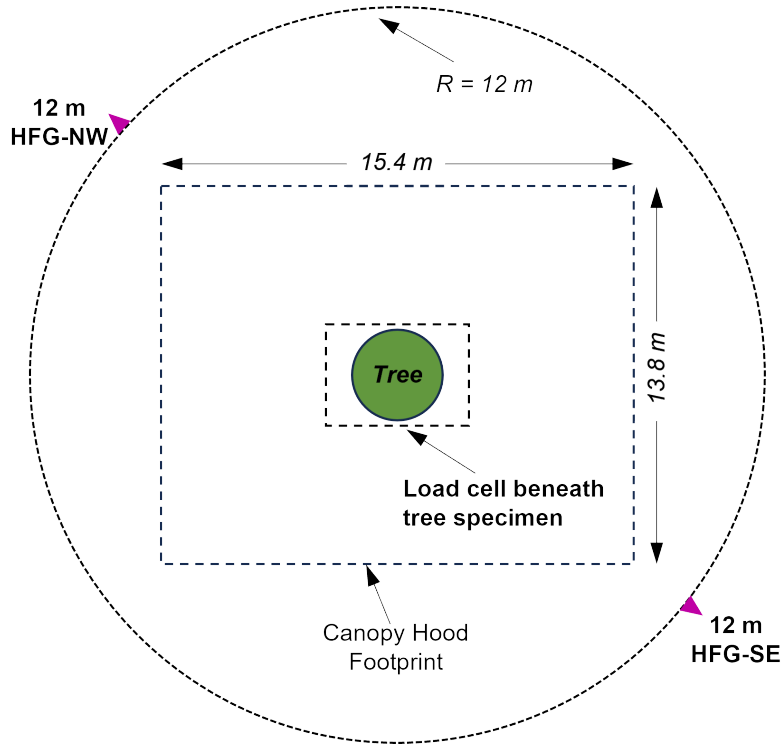


Figure 1: Plan view schematic showing the experimental setup and instrumentation.

study based on their height, which was roughly 4 m (Trees 1 and 2), 4.5 m (Trees 3 and 4), and 6 m (Trees 5 and 6). The trees were stored until they were extremely

dry, and all had a similar moisture content. A description of each of the trees is summarized in Table 1. Although there was natural variation among each pair, Table 1 shows that each pair of trees had similar maximum widths and masses.

A schematic of the experimental setup is shown in Fig. 1. A large round exhaust duct (2.43 m diameter) was located 15.34 m above the floor. Side skirts located 6.44 m above the floor surrounded the canopy hood [5]. The test specimen was placed directly below the center of the exhaust duct. The exhaust flow was adjusted to capture all of the exhaust products and was typically set to 70 kg/s. The trees were mounted on a wood platform and placed on a four-unit load cell system at the center of the exhaust hood area, which recorded the mass throughout the duration of the fire. The measurements discussed below include the transient tree mass using a load cell system, the heat release rate using an oxygen consumption calorimetry system, and the far-field radiative heat flux using water-cooled total heat flux gauges. The instrumentation was connected to a data acquisition system (DAQ) sampling at 1 Hz. A full description of the experimental apparatus and procedures is provided in Ref. [13].

The transient heat release rate (HRR) was determined via oxygen consumption calorimetry achieved by measuring the volume fractions of CO, CO<sub>2</sub>, and O<sub>2</sub> at a well-mixed downstream position in the exhaust duct where the air mass flow rate was carefully measured [5]. A paramagnetic gas analyzer was used to measure the O<sub>2</sub> mass fraction, while non-dispersive infrared (NDIR) gas analyzers were used for the CO and CO<sub>2</sub>.

Water-cooled heat flux gauges (HFG) were placed to the southeast and northwest of the tree at far-field (10 m and 12 m) distances and a height of 2.3 m above the floor (see Fig. 1).

Ignition of the trees was achieved using a natural gas octagonal ring burner positioned below the lowest branches such that its 10 cm to 20 cm flames would impinge on the lowest tree branches. An electronic spark system was used to remotely ignite the ring burner. Prior to the experiments, the ring burner lines were charged with natural gas. The gas flow was turned on about 1 s prior to the spark ignition. The ring burner subsequently ignited the tree and gas flow to the ring burner was maintained for 10 s.

### **3. Time Response**

For practical purposes, most oxygen consumption calorimetry measurement systems, including the NIST system, do not directly correct for instrument response time, because the correction is complex and the argument goes that the difference in

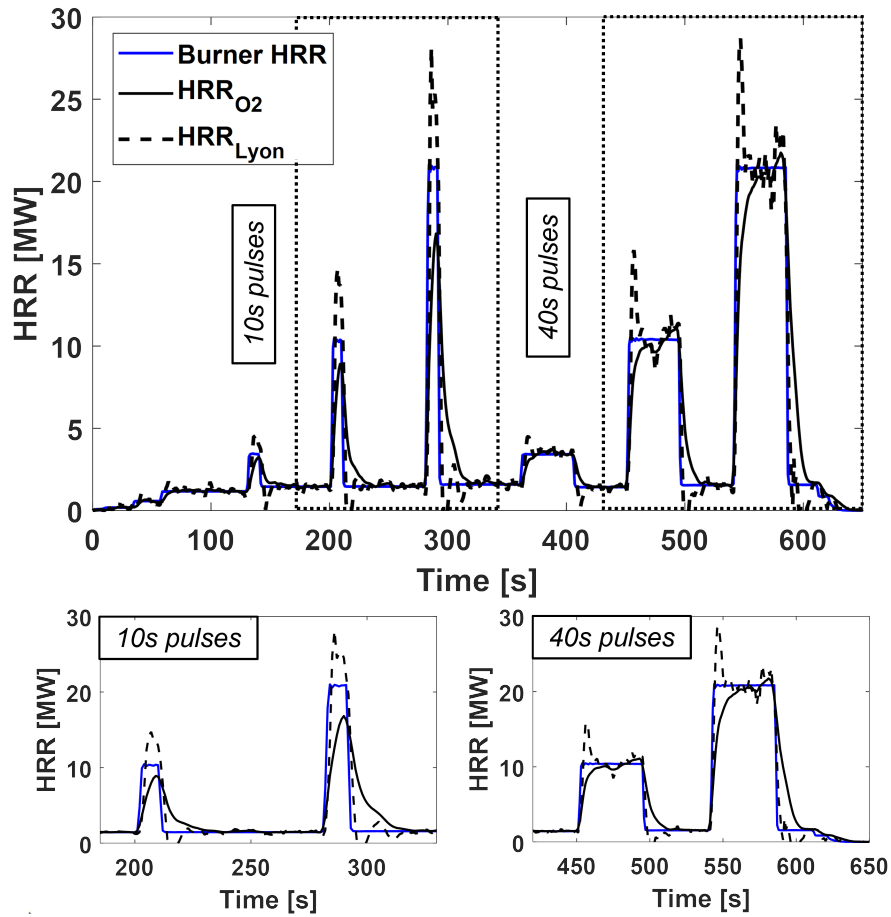


Figure 2: HRR data from confirmation burns using a fast-response natural gas burner. The HRR correction using the method based on Lyon [7] is shown alongside the HRR based on  $O_2$  consumption calorimetry.

the results is small for relatively slow events or relatively fast response times [12]. The calorimetry system response time is primarily a convolution of the individual instrument response times (gas concentrations, temperatures, pressure, etc.). The time constants for the  $CO$  and  $CO_2$  gas analyzers are approximately 4 s and the time constant for the  $O_2$  analyzer is about 2.3 s, while the time constant for the entire calorimetry system is measured as 8 s [5]. These values suggest that the  $O_2$  analyzer is not limiting the system time constant but that other factors strongly influence the system time constant. Mixing of the products of combustion in the canopy hood and duct work, the flow rate of the exhaust system, and the fire size

can all play a role in the system time response. A measurement system with a relatively long response time leads to lower measured values of a signal's rate of change and consequent peak broadening and decreased signal extremes (maxima, minima, and fluctuations). The NIST calorimetry system does consider both the lag time and the delay time as recommended by ASTM [11, 12]. The expanded ( $k = 2$ ) combined uncertainty of the calorimetry system was to be between 5.6 % and 11.3 %, depending on the experimental conditions. Considering that the peak HRR of the fires investigated in this study occurred less than approximately 10 s after ignition (see Table 3), the system response time of 8 s [5] becomes a significant source of uncertainty in the transient results.

A fuel consumption calorimetry system (natural gas burners and flow control) was used to generate precise amounts of heat release in an imposed square-wave shaped applied thermal load, allowing rigorous evaluation of the oxygen consumption calorimetry system, its uncertainty, and its time response. Fig. 2 shows the HRR from a series of calibration burns conducted to assess the accuracy of the O<sub>2</sub> consumption calorimetry system. The calibration burns used a natural gas burner with a pneumatically-actuated v-notch ball valve with a 1 s time constant, generating square-wave shaped heat release rate pulses of various durations. The calibration burner was set to start at 1.0 MW and go as large as 20 MW using the method described in Ref. [5]. The calibration gas composition was measured via gas chromatography such that the HRR based on fuel consumption could be determined (*Burner HRR* in Fig. 2). The *Burner HRR* serves as a baseline for comparison as it has an expanded relative uncertainty of 1.5 % [5]. Also shown is the method developed by Lyon for deconvoluting the HRR data to remove the effect of instrument response time on the transient heat release rate profile [7]. In Lyon's method, the corrected instantaneous heat release rate,  $HRR_{Lyon}(t)$ , is expressed in terms of the measured calorimetric signal,  $HRR_{O_2}(t)$ , as:

$$HRR_{Lyon}(t) = C \left[ HRR_{O_2}(t) + \tau \frac{d(HRR_{O_2}(t))}{dt} \right] \quad (1)$$

where  $C$  is a calibration constant and  $\tau$  is the system response time, as determined during well-controlled natural gas calibration fire experiments.  $C$  is the ratio of the burner HRR set-point to the measured calorimetry value ( $HRR_{Burner}/HRR_{O_2}$ ) during steady-state, which was determined from a 4 set point calibration (1 MW, 3 MW, 10 MW, 20 MW) as 0.993. From the long duration pulses (40 s) in Fig. 2,  $\tau$ , the time constant, that is the time it takes for  $HRR_{O_2}$  to reach 63 % of the steady-state value, was determined to be 8 s.

The short duration pulses (10 s) in Fig. 2 simulate a fast fire, the O<sub>2</sub> consumption

calorimetry ( $HRR_{O_2}$ ) never reach the reference value during the short pulses and the peak values demonstrated significant lag. Although the Lyon method corrects the time response, it ultimately over-predicts the peak value. Furthermore, due to the differential term in Eq. 1,  $HRR_{Lyon}$  exhibits non-physical spikes anywhere there are sharp gradients in the data such as during the increasing and decaying phases of the square wave pulses. This results in the  $HRR_{Lyon}$  reaching negative values in the decaying phase and values 40 % higher than the baseline during the growth phase.

## 4. Results

### 4.1. Fire Spread Observations

The trees burned remarkably fast. Fig. 3 shows the evolution of flame spread from ignition ( $t = 0$  s) to 60 s after ignition during the burning of Tree 6. The time it took for flames to spread and travel from the base of the tree to near the top of the canopy hood during Test 6 was on the order of 8 s, which represents a flame spread rate on the order of 2 m/s. For reference, this is similar to the laminar flame speed of a stoichiometric premixed hydrogen-air flame at ambient conditions [14]. The time from ignition to peak fire heat release rate for Tree 6 was on the order of 5 s to 10 s. The tree fires then diminished over the next 30 s to 40 s. After another 30 s to 60 s, most of the flames self-extinguished and the trees were mostly in a glowing mode with typically only a few lower branches flaming for about a minute. Portions of the tree remnants smoldered for another minute until they completely self-extinguished. Video recordings of the tree fire experiments (along with the calorimetry data) are available for viewing at the NIST Fire Calorimetry Database (FCD) [15].

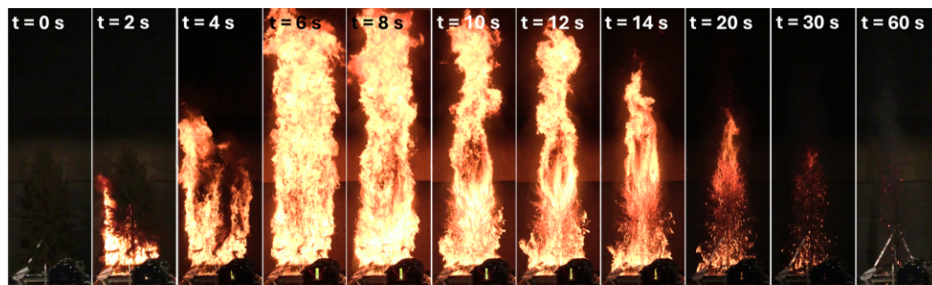


Figure 3: Flame spread evolution of Tree 6 from ignition ( $t = 0$  s) to 60 s after its ignition. Images at 0 s and 60 s have been brightened to show the tree. The camera was positioned 8.7 m away from the tree and angled upwards approximately  $45^\circ$  to capture the entire flame plume.

The character of the tree ignition (symmetric versus non-symmetric) and the degree of igniter flame interaction with the lowest outer branches strongly influenced the fire spread behavior on the tree. A brief description of the ignition character and fire spread is provided in Table 2.

Table 2: Summary of ignition character, fire spread, and other experimental observations.

<b>Tree Ignition Character</b>	<b>Fire Spread Description</b>
1 Non-symmetric.	Burner failed to ignite several lower branches. Significant amount of protracted burning.
2 Nearly symmetric; south half of burner ignited 2 s late.	Despite uneven ignition, most of tree simultaneously ignited. A few lower branches on the southwest and west sides didn't burn.
3 Non-symmetric.	Bottom third of lowest outer branches didn't burn.
4 Nearly symmetric.	A few lower branches didn't ignite. Most of the tree burned.
5 Non-symmetric; south half of burner didn't ignite.	Fire spread more slowly and then downward on the south side. Eventually, most of the tree burned except a few lower outer branches.
6 Nearly symmetric; south half of burner ignited 2 s late.	Nearly all branches consumed. Only one small lower outer branch on the south side remained.

#### 4.2. Heat Flux

Fig. 4 shows the transient far-field heat flux measured by the NW and SE gauges, which were both located at a radial distance of 12 m (see Fig. 1). The gauges yielded similar results except for Trees 1 and 3, for which the ignition process was not perfectly symmetric. For all the trees, the peak heat flux occurred in the first 5 s to 12 s after ignition (time = 0).

#### 4.3. Mass Loss

To obtain the actual mass of tree that burned, the load cell measurements were corrected for the tree foliage moisture content using  $MC_w$  (see Table 1) following Eq. 2. The fuel mass loss ( $m(t)$ ) was estimated by subtracting the specimen's water mass from the measured mass loss ( $m_{measured}(t)$ ):

$$m(t) = m_{measured}(t) \times \underbrace{(1 - MC_w)}_{\text{moisture content correction}} \quad (2)$$

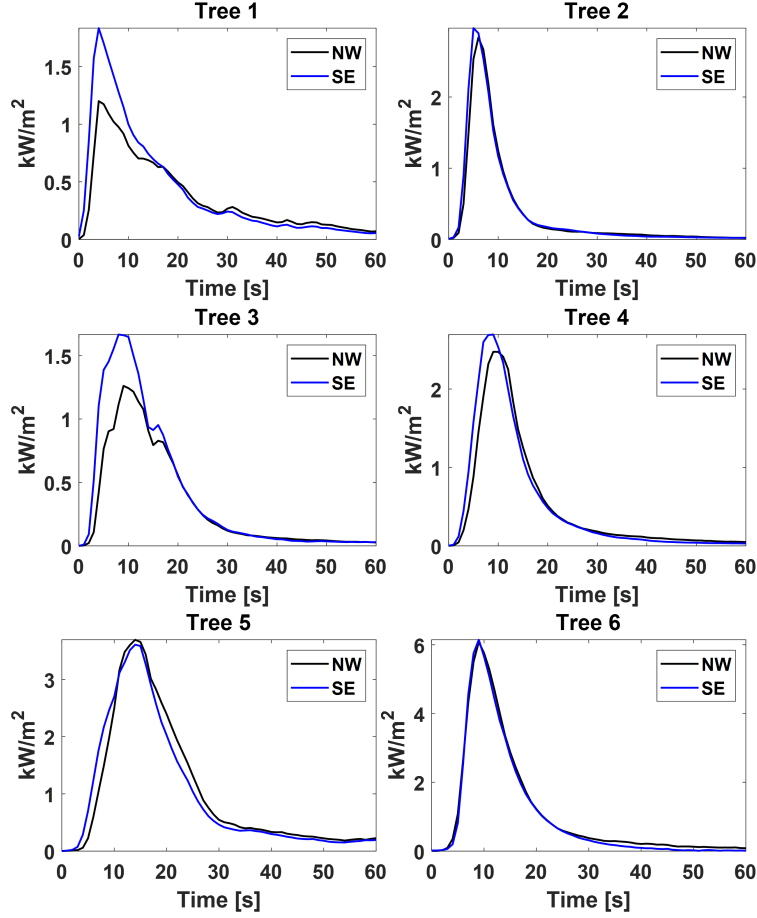


Figure 4: The NW and SE far-field transient heat fluxes measured at a distance of 12 m.

A similar correction is applied to the mass loss rate ( $\dot{m}$ ) and total mass loss ( $\Delta m$ ):

$$\dot{m} = \dot{m}_{measured} \times (1 - MC_w) \quad (3)$$

$$\Delta m = \Delta m_{measured} \times (1 - MC_w) \quad (4)$$

The mass loss rate ( $\dot{m}$ ) was determined by differentiating the transient mass measurement via a central difference scheme and the total fuel mass loss ( $\Delta m$ ) is calculated as the difference between the initial and final masses as measured by the load cell. The post-fire residual tree mass is mainly composed of the tree trunk and unburned branches. The moisture content of the base of the tree trunks was measured from samples extracted immediately before and after the tests. On average,

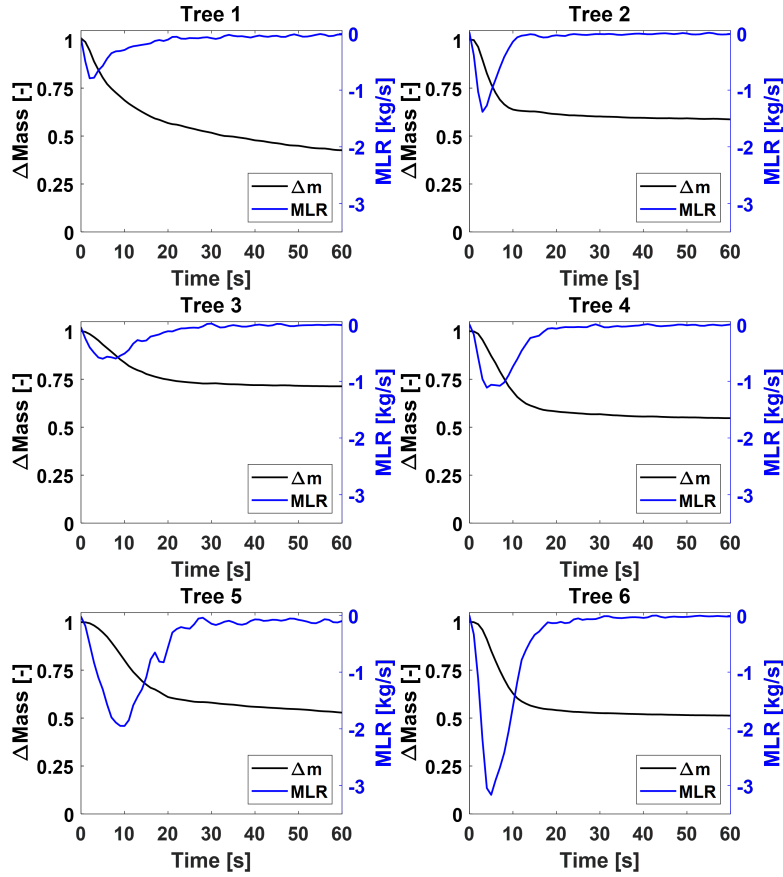


Figure 5: The transient normalized mass measured by the load cell system and the calculated mass loss rate.

the post-fire moisture content of the charred tree trunks was  $21.4 \pm 2.9 \%$ , which was about 3 % lower than their pre-test average moisture content. Considering measurement uncertainty (2.9 %), this difference was interpreted as insignificant. Thus, measurements of the trunk moisture content are consistent with the assumption that the moisture content of the residual mass was essentially unchanged from its initial value (within measurement uncertainty). The water correction term in Eqs. 2 to 4 expresses this idea - that the initial moisture content percentages of both the tree foliage and the tree trunks were invariant during the experiment. The mass loss data (and derived quantities) throughout this study are presented as the moisture corrected values.

Fig. 5 shows the transient mass (normalized by the initial mass) measured by

the load cell system during the tree fire experiments alongside the calculated mass loss rate. In general, most of the mass loss occurred in the first 30 s after ignition (time = 0) and the peak mass loss rate occurred in the first 10 s after ignition. The transient mass loss rates along with the heat flux measurements are used in this study to rescale the calorimetric HRR as discussed below.

#### 4.4. Calorimetry: Transient results

The heat release rate (HRR) was measured in the exhaust hood using the Oxygen consumption ( $O_2$ ) calorimetry methodology outlined by Bryant and Bundy [5]. For comparison, the HRR was also determined using the mass loss rate ( $\dot{m}$ ) such that:

$$HRR_{\dot{m}} = \dot{m} \times H_c \quad (5)$$

where  $\dot{m}$  is the mass loss rate (Eq. 3, Fig. 5) and  $H_c$  is the specified net heat of combustion per unit mass of fuel for Douglas fir, taken as 21 kJ/g following Susott [16] with an estimated uncertainty of 3 % [13].  $HRR_{\dot{m}}$  can be regarded as the idealized heat release rate. Fig. 6 compares the HRR obtained from the mass loss rate ( $HRR_{\dot{m}}$ ; Eq. 5) and the HRR from calorimetry ( $O_2$  consumption) as a function of time after ignition. In all cases, the peak value of the  $HRR_{\dot{m}}$  (Eq. 5) curve had a larger value and occurred earlier than the measurement using  $O_2$  consumption calorimetry. Fig. 6 shows that Trees 1, 3, and 5, which had non-symmetrical ignitions and thereby slightly longer times to burn the entire tree, featured somewhat better agreement between the two methods than Trees 2, 4, and 6, which ignited symmetrically and quickly consumed the flammable portions of the trees. In all cases,  $HRR_{\dot{m}}$  was lower than the  $O_2$  calorimetry HRR during the period after the peak HRR. These phenomena (earlier times to peak, larger peak values, and smaller post-peak values) for the  $HRR_{\dot{m}}$  curves (relative to the calorimetry HRR curves) are attributed to the relatively fast time response of the load cell system compared to the calorimetry instrumentation. Whereas the load cell system had a sub-second time constant, the calorimetry system had an 8 s time constant. A correction method to address the time response of the HRR calorimetry measurement system using load cell and heat flux measurements is discussed below.

#### 4.5. Calorimetry: Time integrated results

The calorimetry results are summarized in Table 3, including the total fuel mass loss corrected for moisture content ( $\Delta m$ ), the residual mass percentage, the peak HRR, the time to peak HRR, and the total heat released (THR). The THR is

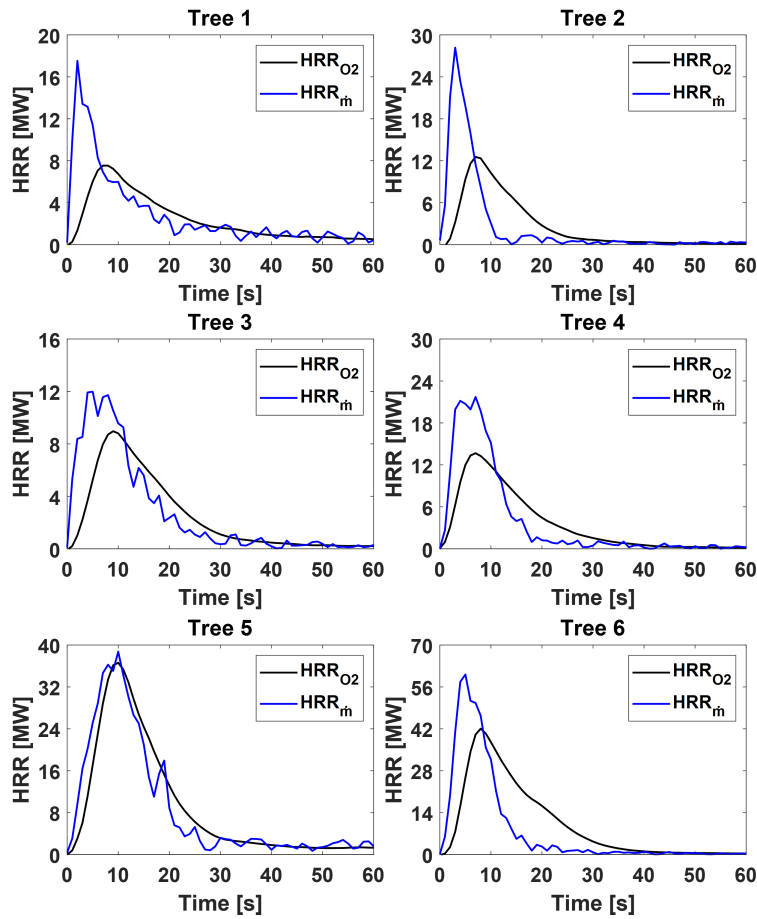


Figure 6: HRR based on  $O_2$  consumption and  $\dot{m}$  for the six tree experiments.

the HRR measured via oxygen consumption calorimetry integrated over the entire test duration. The residual mass ratio is the mass of the specimen that didn't burn divided by the specimen's initial mass.

Fig. 7 compares the total heat released calculated from the  $\dot{m}$  and  $O_2$  consumption HRR methodologies. The dotted line represents parity. For most of the trees (Trees 1 - 5), the difference in heat released between the two methods is less than 10 %. The average difference for all trees is equal to 12 %. Tree 6 showed larger differences with lower THR from the mass loss method. However, despite the differences, Fig. 7 shows that the THR calculated based on the total mass loss and the calorimetry agree within experimental uncertainty.

Table 3: Summary of test results including the fuel mass loss corrected for water content ( $\Delta m$ ), residual mass percentage, peak HRR, time to peak HRR, and the total heat release (THR) along with their respective expanded ( $k=2$ ) combined uncertainties, representing a 95 % confidence interval.

Tree	$\Delta m$ [kg]	Residual mass [%]	Peak HRR [MW]	Time to Peak HRR [s]	THR [MJ]
1	$9.4 \pm 2.5$	35	$7.5 \pm 0.5$	$8 \pm 4$	$169 \pm 12$
2	$7.8 \pm 1.8$	58	$12.5 \pm 0.7$	$7 \pm 4$	$160 \pm 11$
3	$8.2 \pm 2.7$	71	$9.0 \pm 0.5$	$9 \pm 4$	$154 \pm 10$
4	$11.3 \pm 2.7$	54	$13.7 \pm 0.8$	$7 \pm 4$	$218 \pm 15$
5	$28.3 \pm 5.9$	49	$36.6 \pm 2.2$	$10 \pm 4$	$594 \pm 38$
6	$24.4 \pm 5.7$	51	$42.1 \pm 2.6$	$8 \pm 4$	$622 \pm 39$

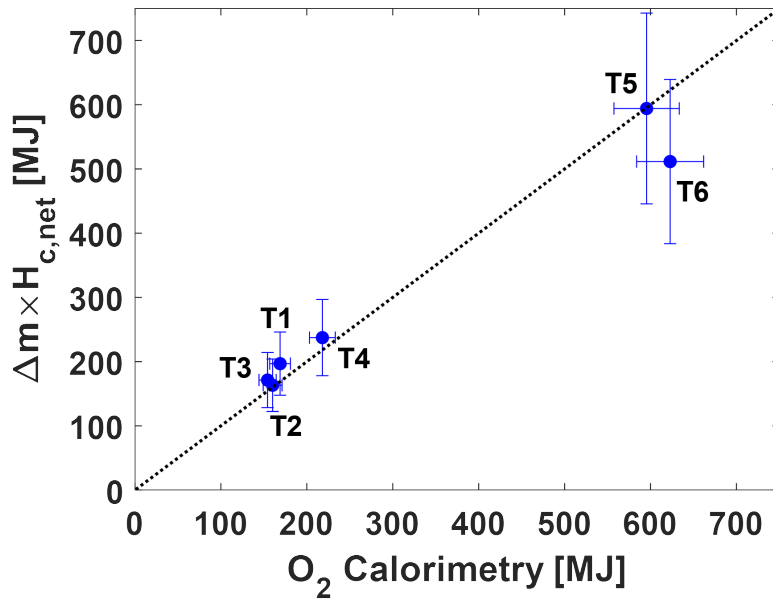


Figure 7: The total heat released determined from the total mass loss (Eq. 5) versus the O<sub>2</sub> consumption calorimetry. The dotted line represents parity, and the error bars represent the expanded combined uncertainties, representing a 95 % confidence interval.

## 5. Rescaling HRR Method

The effect of the calorimetry system time response (as discussed with regard to Fig. 6) resulted in peaks from the O<sub>2</sub> consumption measurement that are smaller and

broader than the  $\dot{m}$  derived HRR. In contrast to a calorimetry system, the water-cooled heat flux gauges and the mass load cell system used here are relatively fast. The Huskeflex SGB01 thermal heat flux sensors have a time constant of 450 ms [17], which indicates that 89 percent of the true signal is recovered at a 1 Hz sampling interval - about 20 times faster than the calorimetry system. Strain gauge type devices such as the load cell have a very fast time response, typically on the order of 1 ms. The THR, as a time-integrated measurement, is agnostic to the time response. Leveraging this fact, the HRR profiles are corrected for time response by matching the shapes of the profiles derived from the fast-responding instruments (heat flux and mass load cell), and imposing the requirement that the measured total heat released (THR) matches the value obtained from oxygen consumption calorimetry. The rescaled HRR profiles based on the transient profiles of heat flux and mass loss rate ( $HRR'_q(t)$  and  $HRR'_{\dot{m}}(t)$ , respectively) were determined using the following equations:

$$HRR'_q(t) = 4\pi R^2 \overline{q''}(t) \times K_q \quad (6)$$

$$HRR'_{\dot{m}}(t) = \dot{m}(t) \times K_m \quad (7)$$

where  $\overline{q''}$  is the average far-field heat flux obtained from the two gauges,  $R$  is the distance of the heat flux gauges from the tree's central axis, and  $\dot{m}$  is the mass loss rate obtained by differentiating the mass data from the load cell. The rescaling factors  $K_q$  and  $K_m$  are defined as:

$$K_q = \frac{\int_{t_i}^{t_e} HRR(t) dt}{4\pi R^2 \int_{t_i}^{t_e} \overline{q''}(t) dt} = \frac{THR}{TRE}, \quad (8)$$

$$K_m = \frac{\int_{t_i}^{t_e} HRR(t) dt}{\int_{t_i}^{t_e} \dot{m}(t) dt} = \frac{THR}{\Delta m}. \quad (9)$$

Here, the integrals are over the entire duration of the fire, from the time of ignition,  $t_i$ , until the time when flames and smoldering extinguish,  $t_e$ . The heat flux rescaling factor,  $K_q$ , is the ratio of the total heat released (THR) to the average total radiated energy (TRE) and the mass loss rate rescaling factor  $K_m$  is the ratio of the total heat released (THR) to the moisture content corrected mass loss ( $\Delta m$ ). The ratio

( $THR/\Delta m$ ) is referred to as the net effective heat of combustion in the NIST Fire Calorimetry Database (FCD) [15]. Both rescaling factors ( $K_q$  and  $K_m$ ) are time invariant.

Fig. 8 revisits a short and long pulse from the natural gas calibration experiments shown in Fig. 2 with the rescaled HRR based on the transient heat flux profile,  $HRR'_q(t)$  (Eq. 6) added for comparison. The figure shows the idealized natural gas burner HRR (*Burner HRR*), the HRR based on  $O_2$  consumption calorimetry ( $HRR_{O_2}$ ), and the HRR correction based on the Lyon [7] method ( $HRR_{Lyon}$ ) in comparison to the rescaled HRR based on Eq. 6. The rescaled HRR profile closely follows the ramp-up and ramp-down of the burner HRR, falls within about 10 % of the burner's (large) steady value, and corrects rounding due to the calorimetry system's time constant at the edges of the thermal square-shaped wave. The rescaled profile is somewhat lower before (time < 540 s) and after (time > 590 s) the main natural gas pulse as might be expected for the large (1 m x 2 m) natural gas burner, which provides a fire that is large in area, but small in height such that the view factor of the radiometers is relatively small. The rescaled profile does not exhibit the overshoot and undershoot of the Lyon method [7]. The data from Fig. 8 confirms that the heat flux based rescaling method (Eq. 6) can provide accurate results of HRR. Unfortunately, a similar confirmation experiment for the  $\dot{m}$  method (Eq. 7) has yet to be performed as a large square-wave thermal pulse is more challenging to achieve with a solid fuel.

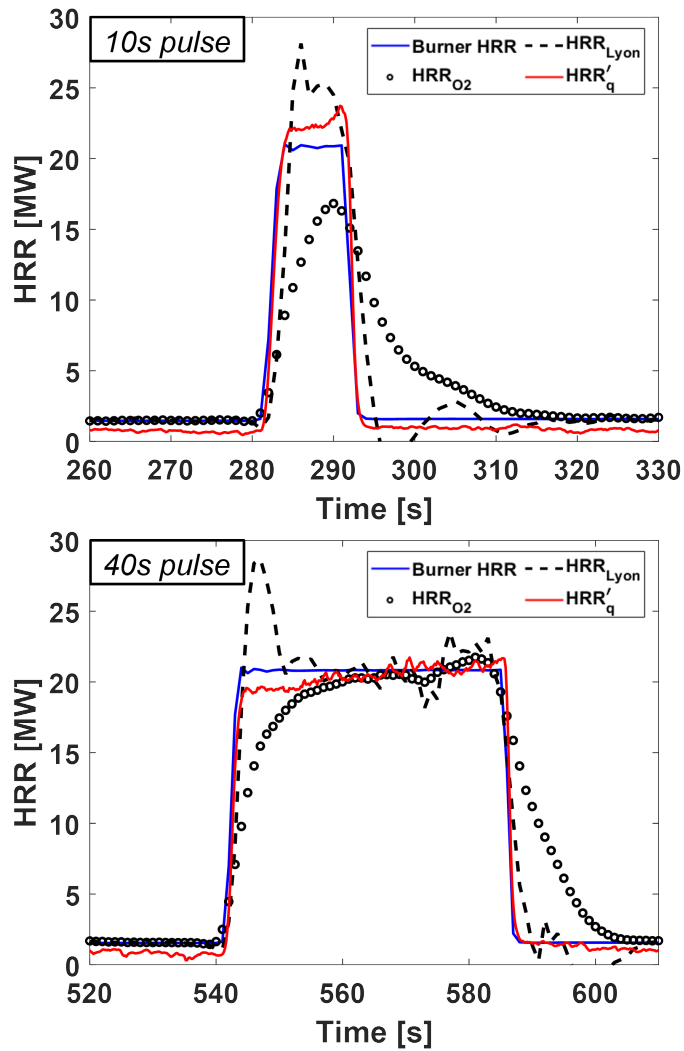


Figure 8: Rescaled transient HRR profile,  $HRR'_q$ , compared to the original calorimetric  $O_2$  and the Lyons correction for a short (top) and long pulse (bottom) square wave shaped natural gas calibration burn.

Each of the rescaling approaches requires assumptions about the fire and therefore limitations in their application. For the rescaled HRR based on the heat flux profile ( $HRR'_q(t)$ ), it is assumed that the radiative fraction is constant as a function of time (and implicitly, as a function of HRR) during the fires. It is also assumed that smoke and gas absorption does not significantly reduce the measured radiative signal intensity, and that the entire fire is unobscured and visible by the heat flux

gauge. Although the heat flux gauges have a large view factor at such a far distance (12 meter), physical obstructions from the tree itself can obscure portions of the fire. Finally, although the background radiation is accounted for initially, it is assumed that it did not significantly increase due to these short duration fires.

The rescaled HRR based on the mass loss rate profile ( $HRR'_m(t)$ ) assumes that all combustion occurs with the foliage attached to the tree. Of course, the gas phase combustion is not instantaneous even for foliage attached to the tree. The gas phase combustion is delayed and effectively smeared approximately by the combustion residence time of a fuel packet in the fire plume, which is on the order of 1 s to 3 s. Such behavior is analogous to a similarly large, natural gas fire. Burning in such a fire occurs over the entire fire volume as fuel travels upward. Since natural gas fires were used to calibrate the oxygen calorimetry system, these effects are not regarded as a strong influence on the HRR results seen in Fig. 9. The more salient issue to consider are the embers and firebrands that are observed to detach from the trees and burn while being lofted upwards. Yet, experimental observations and the video record suggest that the number of firebrands is very small, so the delay and smearing of the recalculated HRR results based on the mass loss measurements (see discussion below regarding Fig. 9) is considered negligible. The  $HRR'_m(t)$  also assumes that the combustion efficiency is invariant during the burn, and that the moisture content of the tree is constant during burning. Additionally, the effects of smoldering are negligible as minimal smoldering was observed, and a constant heat of combustion is assumed throughout the tree fire. Finally, any buoyancy effects experienced by the tree are neglected and assumed to not impact the transient load cell measurement. A computational fluid dynamic fire model of the Douglas-fir tree experiments using FDS 6.9.1 [18] shows that the drag force is finite and that it changes with time as the tree burns away and the velocity field changes. The drag force is zero when there is no buoyancy induced flow at the start and end of the fire. As the fire starts, the buoyant plume generated by the fire interacts with the foliage and branches producing a drag force that reduces the mass loss measurement. The drag force increases with the increase in buoyant flow, with estimated peak values on the order of 1 kgf (or 10 N) for the fires considered here. The force decreases as both the foliage burns away and the induced flow decreases. Whereas the maximum velocity occurs at the time of peak heat release, the maximum foliage surface area is at the start of the test. Thus, the drag may shift the measured mass loss profile and the calculated maximum of the mass loss rate (and peak heat release rate of the rescaled HRR profile). Of course, modeling a tree fire, and the associated transient buoyancy force is pioneering work. The effects of these assumptions on  $HRR'_q(t)$  and  $HRR'_m(t)$  are complex

due to measurement and modeling uncertainties.

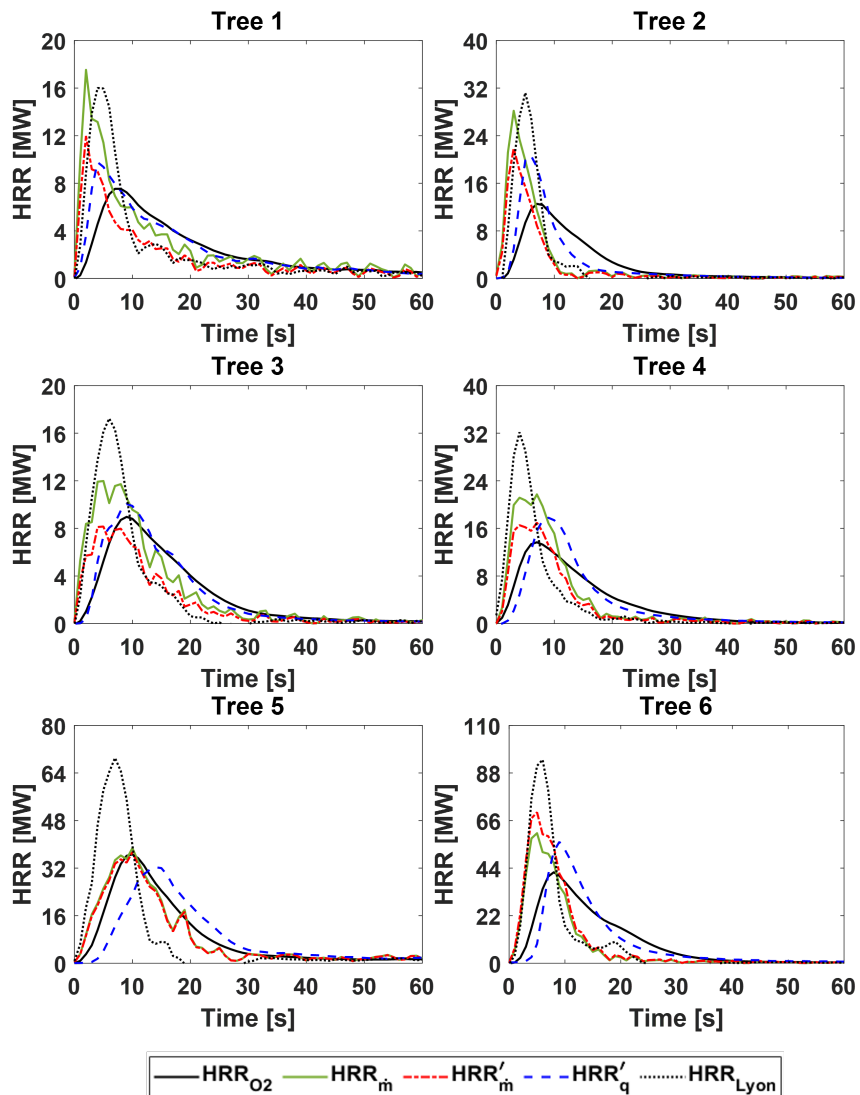


Figure 9: Rescaled transient HRR profiles compared to the original O<sub>2</sub> consumption calorimetry and  $\dot{m}$  based measurements for all of the trees.

### 5.1. Rescaling Results and Discussion

The rescaled HRR profiles ( $HRR'_q$  and  $HRR'_m$ ) are shown in Fig. 9 alongside the original O<sub>2</sub> consumption calorimetry ( $HRR_{O_2}$ ) and  $HRR_m$  (the mass loss rate

derived HRR profile from Eq. 5). As expected, the rescaled peaks are generally narrower and larger than the profiles measured by calorimetry.

The peaks of  $HRR'_m$  follow the trends seen in Fig. 7 (where the divergence from the parity line is proportional to the difference between the peaks of HRR based on  $\dot{m}$  and  $O_2$  consumption) as well as the shapes of the  $\dot{m}$  profiles themselves. The shapes of the  $HRR_m$  and the  $HRR'_m$  profiles are identical, with their values differing at all times by the ratio of  $H_c/(THR/\Delta m)$  (derived from the ratio of Eq. 5 to Eq. 7).

The uncertainty in the peak  $HRR'_m$  is related to the uncertainties in the THR and the total mass loss measurement (24 % on average; see Table 4), as well as the estimated errors in the central differencing scheme used to calculate  $\dot{m}$  from the load cell measurements (43 % on average), which dominates the relative uncertainty. The large value of the latter contributor to the uncertainty can be attributed to the relatively slow data sampling rate (1 Hz) compared to the relatively rapid change in the mass loss rate. Further, the error in the central differencing scheme is proportional to the square of the time step of the data and the truncation error in the Taylor series. In retrospect, increasing the data acquisition rate by an order of magnitude would have significantly reduced the uncertainty of this term for these short duration tree burns.

The profiles from the two far-field (12 m) heat flux gauges (see Fig. 4) were averaged and used to rescale the HRR profile according to Eq. 6. In most cases,  $HRR'_q$  resulted in a higher peak HRR and faster time to peak HRR. The response time of the heat flux gauges is sub-second, however, due to the sampling frequency, it is effectively constrained to 1 s. Additionally, the  $HRR_{O_2}$  results are time shifted within the data processing already implemented within NFRL from the response of a separate heat flux gauge deployed during all experiments [5]. For this reason, the time to peak results do not improve significantly between  $HRR_{O_2}$  and  $HRR'_q$ . However, the time-response was improved as evident by the narrower peaks of  $HRR'_q$  compared to those of  $HRR_{O_2}$ . The  $HRR'_q$  results of the symmetric tree fires (Trees 2, 4, 6) showed the greatest time-response improvement as those fires were relatively faster than the non-symmetric ignitions. Additionally, as the fire size grows, the assumption that the heat flux gauges views the entire fire breaks down. Lyon's method ( $HRR'_m$ ) is also shown in Fig. 9. Unsurprisingly, its peak occurs within a second or two of the rescaled  $HRR'_m$ , and is earlier and larger than the  $HRR_{O_2}$  curves. This is presumably due to the overshoot of the peak as indicated by implementation of Lyon's method for the natural gas calibration fire as seen in Fig. 8. The peak HRR and time to peak HRR from both of the rescaling approaches ( $HRR'_m$  and  $HRR'_q$ ) are presented in Table 4, alongside the

results from O<sub>2</sub> calorimetry. The uncertainty of the peak  $HRR'_q$  is related to the relative uncertainties in THR (6 % on average; see Table 4) and TRE (14 % on average), as well as the range of results associated with averaging the far-field heat flux measurements (12 % on average).

Table 4: The Peak HRR and the time to peak HRR measured by calorimetry and from the rescaled results using Eq. 7 ( $HRR'_m$ ) and Eq. 6 ( $HRR'_q$ ) and their respective expanded (k=2) combined uncertainties, representing a 95 % confidence interval. The calorimetric THR is also listed.

Tree	O <sub>2</sub> Calorimetry			$HRR'_m$		$HRR'_q$	
	Peak HRR [MW]	Time to Peak HRR [s]	THR [MJ]	Peak HRR [MW]	Time to Peak HRR [s]	Peak HRR [MW]	Time to Peak HRR [s]
1	7.5 ± 0.5	8 ± 4	169 ± 12	11.9 ± 8.6	2 ± 2	9.8 ± 3.3	5 ± 2
2	12.5 ± 0.7	7 ± 4	160 ± 11	22.0 ± 14.4	3 ± 2	20.6 ± 3.2	6 ± 2
3	9.0 ± 0.5	9 ± 4	154 ± 10	8.2 ± 4.8	5 ± 2	10.0 ± 2.8	8 ± 2
4	13.7 ± 0.8	7 ± 4	218 ± 15	16.9 ± 10.3	7 ± 2	17.8 ± 3.0	8 ± 2
5	36.6 ± 2.2	10 ± 4	594 ± 38	37.4 ± 12.6	10 ± 2	32.3 ± 4.8	12 ± 2
6	42.1 ± 2.6	8 ± 4	622 ± 39	69.8 ± 26.5	5 ± 2	56.1 ± 8.3	6 ± 2

The rescaled  $HRR'_m$  resulted in peak HRRs that were on average 36 % higher than the  $HRR_{O_2}$  while  $HRR'_q$  had peak HRRs that were, on average, 26 % higher than  $HRR_{O_2}$ . Likewise, the time to peak was reduced by an average of 3 s and 0.7 s, respectively, for the  $HRR'_m$  and  $HRR'_q$  re-scalings. As expected, in most cases the time to peak was as fast or faster than  $HRR_{O_2}$ .

The rescaled peak HRRs ( $HRR'_m$  and  $HRR'_q$ ) differed from each other by an absolute value of 15 % on-average, always with overlapping uncertainties. The times to peak HRR of the rescaled HRR profiles was always shorter for  $HRR'_m$ , differing by 2.2 s on average. This difference in the times to peak HRR can be understood in terms of the limitations of the rescaled HRR ( $HRR'_m$ ) for which combustion does not instantaneously occur in proportion to the rate of tree mass loss (see above).

## 6. Conclusions

The NIST large-scale O<sub>2</sub> consumption calorimetry system is capable of accurately resolving fire events with a peak lasting longer than about 20 s. The rapidly growing Douglas fir tree fires considered in this study, however, pushed the limits of the system. Due to the time response of the system and the relatively fast growing fires, there was peak broadening of the measured HRR, where the peak HRR was under-reported while post peak measurements were over-reported. In this study, the O<sub>2</sub> calorimetry HRR profiles were corrected for the calorimetry

system time response. The total heat released measured by the O<sub>2</sub> calorimetry system is rescaled using the shapes of the profiles derived from relatively fast-responding instruments (heat flux and mass load cell) with the condition that the total heat released by the rescaled HRR curves match the time-integrated total heat released as measured by the O<sub>2</sub> calorimetry HRR system over the entire experimental duration. This is a generalizable approach based on the calorimetry system measurement itself.

The rescaled profiles feature higher peak HRRs and faster times to peak HRR, as well as overall narrower peaks, while maintaining the same total heat released measured by the O<sub>2</sub> consumption calorimetry system. Although each of the rescaling methods are limited by many assumptions and approximations, a test of the  $HRR'_q$  rescaling method yielded a HRR profile within about 10 percent of the natural gas burner's peak thermal output. The  $HRR'_m$  rescaling method based on the load cell measurement yielded comparable peak values to the  $HRR'_q$  rescaling method based on the far field radiometer measurement, differing by an absolute value of 15 % on-average and with overlapping uncertainties. These methodologies provide a simple way to correct calorimetry measurements in rapidly growing fires through the use of supplementary measurements of mass loss or heat flux, which are commonly used in fire laboratories.

## Acknowledgments

The authors are grateful to Artur Chernovsky, Anthony Chakalis, Phil Dear-dorff, Marco Fernandez, and Justin Mills for their indispensable assistance.

## References

- [1] V. Babrauskas, R. D. Peacock, Heat release rate: The single most important variable in fire hazard, *Fire Safety Journal* 18 (3) (1992) 255–272. doi:doi.org/10.1016/0379-7112(92)90019-9.
- [2] C. Huggett, Estimation of rate of heat release by means of oxygen consumption measurements, *Fire and Materials* 4 (2) (1980) 61–65. doi:doi.org/10.1002/fam.810040202.
- [3] P. A. Enright, C. M. Fleischmann, Uncertainty of Heat Release Rate of the ISO56601 Cone Calorimeter Standard Test Method, *Fire Technology* 35 (1999) 153–169. doi:doi.org/10.1023/A:1015416005888.

- [4] R. A. Bryant, G. W. Mulholland, A guide to characterizing heat release rate measurement uncertainty for full-scale fire tests, *Fire and Materials* 32 (3) (2008) 121–139. doi:doi.org/10.1002/fam.959.
- [5] R. A. Bryant, M. F. Bundy, The NIST 20 MW calorimetry measurement system for large-fire research, Tech. Rep. NIST TN 2077, National Institute of Standards and Technology, Gaithersburg, MD (Dec. 2019). doi:10.6028/NIST.TN.2077.
- [6] D. Evans, L. Breden, Time delay correction for heat release rate data, *Fire Technology* 14 (1978) 85–96. doi:doi.org/10.1007/BF02308904.
- [7] R. E. Lyon, A. Abramowitz, Effect of instrument response time on heat release rate measurements, *Fire and Materials* 19 (1) (1995) 11–17. doi:10.1002/fam.810190103.
- [8] B. Messerschmidt, P. Van Hees, Influence of delay times and response times on heat release measurements, *Fire and Materials* 24 (2) (2000) 121–130. doi:10.1002/1099-1018(200003/04)24:2<121::AID-FAM732>3.0.CO;2-K.
- [9] W. M. Pitts, Applied Heat Flux Distribution and Time Response Effects on Cone Calorimeter Characterization of a Commercial Flexible Polyurethane Foam, *Fire Technology* 50 (3) (2014) 635–672. doi:10.1007/s10694-011-0235-8.
- [10] P. A. Croce, A Method for Improved Measurement of Gas Concentration Histories in Rapidly Developing Fires, *Combustion Science and Technology* 14 (4-6) (1976) 221–228. doi:10.1080/00102207608547530.
- [11] R. Bryant, E. Johnsson, G. Mulholland, Characterizing heat release rate transients, *Fire Safety Journal* 51 (2012) 126–132. doi:10.1016/j.fire saf.2012.04.002.
- [12] ASTM International (2024), ASTM E2067-24 - Standard Practice for Full-Scale Oxygen Consumption Calorimetry Fire Tests, ASTM International, West Conoshoken, PA, USA. doi:10.1520/E2067-24.
- [13] E. Johnsonn, G. Di Cristina, E. Mueller, M. Bundy, T. Chakalis, M. Fernandez, A. Hamins, The burning characteristics of 3 m to 6 m dry douglas-fir

- trees, Tech. Rep. NIST TN 2327, National Institute of Standards and Technology, Gaithersburg, MD (Jan. 2025). doi:doi.org/10.6028/NIST.TN.2327.
- [14] S. R. Turns, *An Introduction to Combustion: Concepts and Applications*, 2nd Edition, McGraw Hill, 2000.
- [15] M. Bundy, R. Bryant, NIST Fire Calorimetry Database (FCD) (Nov. 2020). doi:10.18434/MDS2-2314.
- [16] R. A. Susott, Characterization of the thermal properties of forest fuels by combustible gas analysis, *Forest Science* 28 (1982) 404–420.
- [17] Huskeflex thermal sensors, SBG01 water-cooled heat flux sensor technical information sheet.  
URL [https://www.hukseflux.com/uploads/product-documents/SBG01\\_v2313.pdf](https://www.hukseflux.com/uploads/product-documents/SBG01_v2313.pdf)
- [18] K. B. McGrattan, R. McDermott, M. Vanella, E. Mueller, S. Hostikka, J. Floyd, *Fire dynamics simulator (6.9.1): User’s guide*, Tech. Rep. NIST SP 1019, National Institute of Standards and Technology, Gaithersburg, MD, 6th ed. (Apr. 2024).  
URL <https://pages.nist.gov/fds-smv/manuals.html>